Available online at www.sciencedirect.com
ScienceDirect
Journal of Solid State Chemistry 180 (2007) 661–669
JOURNAL OF SOLID STATE CHEMISTRY
www.elsevier.com/locate/jssc

$Bi_{2n+4}Mo_nO_{6(n+1)}$ with $n = 3, 4, 5, 6$: A new series of low-temperature stable phases in the $mBi_2O_3 - MoO_3$ system ($1.0 < m < 1.7$): Structural relationships and conductor properties

Eladio Vila[a], Ángel R. Landa-Canovas[a,*], Jean Galy[b], Juan E. Iglesias[a], Alicia Castro[a]

[a]*Instituto de Ciencia de Materiales de Madrid, CSIC, Cantoblanco, 28049 Madrid, Spain*
[b]*Centre d'Elaboration de Matériaux et d'Etudes Structurales, CNRS, 29 rue Jeanne Marvig, B.P. 94347, 31055 Toulouse Cedex 4, France*

Received 8 September 2006; received in revised form 24 October 2006; accepted 25 October 2006
Available online 16 November 2006

Abstract

Four low-temperature phases with compositions $Bi_{10}Mo_3O_{24}$, $Bi_6Mo_2O_{15}$, $Bi_{14}Mo_5O_{36}$ and $Bi_8Mo_3O_{21}$ have been prepared by the *n*-butylamine wet synthesis method. They have been characterized by powder X-ray diffraction and transmission electron microscopy, mainly by selected area electron diffraction. The four phases present a close structural relationship and a common basic fluorite-type structure and are members of a homologous series of phases with general formula $Bi_{2n+4}Mo_nO_{6(n+1)}$, being $n = 3$, 4, 5 and 6, respectively. The matrices relating their superstructures and the basic fluorite type unit cell are given, as well as a general one for the whole series. The conductor behavior of these phases is characterized by impedance spectroscopy being all these materials very good ionic conductors.

Keywords: Bismuth–molybdenum oxides; Fluorite; Structure; Ionic conductors

1. Introduction

Materials belonging to the fluorite structural type have attracted considerable interest owing to their electrical properties, mainly as ionic conductors. One of the best-known oxygen–ion conductors is the high-temperature form of Bi_2O_3 (δ polymorph), which crystallizes with a fluorite structure. Several studies have been focused on the search for new families of oxygen conductors, structurally related to the fluorite framework, in order to develop materials with improved characteristics. Among these, the systems Bi_2O_3–V_2O_5, Bi_2O_3–Nb_2O_5 and Bi_2O_3–Ta_2O_5 have been extensively investigated in the whole range of compositions [1–3]. The Bi_2O_3-rich ends in these systems have been shown to contain several single phases and solid solutions, all of them exhibiting fluorite-type superlattices [4–6]. Probably the richest system, where many fluorite-related phases can be prepared, is Bi_2O_3–MoO_3. This system has been thoroughly studied for the good catalytic properties of its phases, such as in the ammoxidation of alkenes or the oxidation of hydrocarbons [7–9]. Many phases are known in this system [10–18], all of them also related to the fluorite prototype [19], with the exception of the low-temperature polymorph of Bi_2MoO_6 (*L* phase) that exhibits an Aurivillius-type structure, where $[Bi_2O_2]$ and perovskite-like layers alternate in the framework [20]. This Bi_2MoO_6 phase is related with $Bi_4V_2O_{11}$ and $Bi_4V_2O_{10}$, as demonstrated by Galy and coworkers [21].

In general, the synthesis of all these oxides is carried out via the conventional ceramic route, which requires relatively high temperatures, implying that low-temperature stable phases cannot be isolated. In order to avoid this problem, alternative synthesis methods have been tested, such as mechanosynthesis or soft-wet chemistry methods. With regard to conducting materials, the former method has favored the preparation of several ionic conductors [22–24], cathode materials [25] or superconducting oxides [26]. Recently, the authors have reported the existence of two new single phases (low-temperature form

*Corresponding author. Fax: +34 91 372 06 23.
E-mail address: landa@icmm.csic.es (A.R. Landa-Canovas).

0022-4596/$ - see front matter © 2006 Elsevier Inc. All rights reserved.
doi:10.1016/j.jssc.2006.10.036

of $Bi_6Mo_2O_{15}$ [27] and $Bi_{10}Mo_3O_{24}$ [28]), belonging to the Bi_2O_3–MoO_3 system, with very close Bi/Mo ratio, 3 and 3.33, respectively. Both phases are only stable at low temperature, and are structurally related to the so-called $[Bi_{12}O_{14}]$ columnar structural-type illustrated by the $Bi[Bi_{12}O_{14}][MoO_4]_4[VO_4]$ phase, discovered in the Bi–V–Mo–O system and structurally established by Enjalbert et al. [16]. All these phases exhibit a fluorite type sublattice for the heavy atoms. These low-temperature phases can be isolated by means of a wet-chemistry synthesis procedure, different from coprecipitation, which allows nanosized precursors to be prepared. Both L-$Bi_6Mo_2O_{15}$ and $Bi_{10}Mo_3O_{24}$ turn out to be promising ionic-conductor materials.

This paper reports on the careful prospecting of the system mBi_2O_3–MoO_3 ($1.0 \leqslant m \leqslant 1.7$). Other as yet not described oxides with compositions $Bi_8Mo_3O_{21}$ and $Bi_{14}Mo_5O_{36}$, also stable at low temperatures, are obtained as single phases. Their structural characterization was carried out by means of powder X-ray diffraction and electron diffraction (transmission electron microscopy). A tentative relationship between the fluorite framework and the superlattices in these phases in this region of Bi_2O_3–MoO_3 system is established. Finally, the conductor behavior of these materials was measured and compared.

2. Experimental section

Using the so-called *n*-butylamine procedure, previously reported to prepare $Bi_6Mo_2O_{15}$ [27] and $Bi_{10}Mo_3O_{24}$ [28], ten stoichiometric mixtures of $Bi(NO_3)_3 \cdot 5H_2O$ and MoO_3 were employed for the synthesis of reactive precursors, for mBi_2O_3–MoO_3 compositions ranging between $m = 1.0$ and 1.7. These precursors were prepared by adding the amount of MoO_3 (Merck, analytical grade) required to obtain Bi/Mo molar ratios to 0.03 mole of $Bi(NO_3)_3 \cdot 5H_2O$ dissolved in 10 mL of HNO_3 (65% concentration), to which 200 mL of distilled water were added under continuous stirring. The precursor materials were obtained by precipitation of Bi^{3+} cation by dropwise addition (2 mL min^{-1}) of 1 M solution of *n*-butylamine at room temperature, under vigorous stirring, to pH~9.5. Then, these suspensions were filtered, and the precipitates thoroughly washed with distilled water and dried at 80 °C. The composition of the mother liquid was analyzed by inductively coupled plasma (ICP) emission spectroscopy, using a Perkin-Elmer Plasma 40. The solid precursors were annealed at increasing temperatures, for 6 h each, in cumulative treatments, to the complete formation of crystalline phases. Each treatment was finished by cooling inside the furnace.

The evolution of the reactions was followed by X-ray powder diffraction (XRD) on a Philips X'Pert diffractometer, fitted with a Ge(111) incident beam monochromator of the Johansson symmetric type, using Cu$K\alpha_1$ radiation ($\lambda = 1.5405929$ Å). Data were recorded between 5° and 70° (2θ), with 2θ increments of 0.02° and counting time of 1 s per step.

For the determination of the lattice parameters of $Bi_8Mo_3O_{22}$ and $Bi_{14}Mo_5O_{36}$, patterns from 5° to 70° (2θ) were measured at 22 °C using the above mentioned Philips X'Pert diffractometer. The data were taken with a 0.25° divergence slit, an antiscatter slit of 1°, a receiving slit of 0.05 mm, and a set of Soller slits with an axial divergence of $\approx 1.1°$ in the diffracted beam path. The usual $\theta/2\theta$ mode was used, and intensity was counted at steps of 0.01° for 20 s. The flat sample was spun around its normal at about 2 Hz. A second trace was obtained under the same conditions and reduced 2θ domain, with a small amount of NIST Si standard (Standard Reference Material 640b, $a = 5.430940$ Å for the wavelength quoted above) mixed with the sample material, for calibration purposes. Peak positions were determined by hand, with the help of software developed by one of us (E. Vila).

The determination of the volumic mass of the new isolated phase was carried out with an Accupyc 1330 pycnometer using the helium displacement technique.

The particle size and morphology of the single phases, annealed at different temperatures, were investigated by scanning electron microscopy (SEM). The images were taken in the range of 10–20 kV in a Digital Scanning Microscope DSM 960 Zeiss. For this purpose, dispersed particles were placed on a carbon film and a gold layer was sputtered onto the powder samples.

All single phases $Bi_8Mo_3O_{22}$, $Bi_{14}Mo_5O_{36}$, $Bi_6Mo_2O_{15}$ and $Bi_{10}Mo_3O_{24}$ were studied by transmission electron microscopy. Specimens for TEM observations were prepared from suspensions ultrasonically dispersed in butanol. A drop of each corresponding suspension was placed on a copper grid covered with a holey carbon film. A JEM 2000FXII electron microscope, was employed to explore the reciprocal lattice of the samples (double-tilt specimen holder: ±45°) and to obtain medium resolution images.

Electrical conductivity measurements of $Bi_8Mo_3O_{22}$ and $Bi_{14}Mo_5O_{36}$ were carried out by complex impedance spectroscopy with the apparatus described elsewhere [29]. Pellets about 8 mm in diameter and 3 mm in thickness were prepared by spark plasma sintering (SPS), in 5 min at temperatures ranging beteween 600 and 650 °C, depending on the thermal stability of both phases, under a pressure of 75 MPa. These pellets, thinned and polished, with a relative density bigger than 98% in all the cases, were used for electrical measurements.

3. Results and discussion

The precursors obtained by the *n*-butylamine method are a mixture of a very crystalline MoO_3 oxide together with an amorphous phase of the bismuth components. The compositions of all these precursors maintain exactly the Bi/Mo starting ratio, since traces of neither cations were detected by ICP analysis in the separated mother liquids.

The thermal evolutions of the precursors were followed by XRD on samples annealed at different temperatures. Fig. 1 shows the XRD patterns of each product obtained

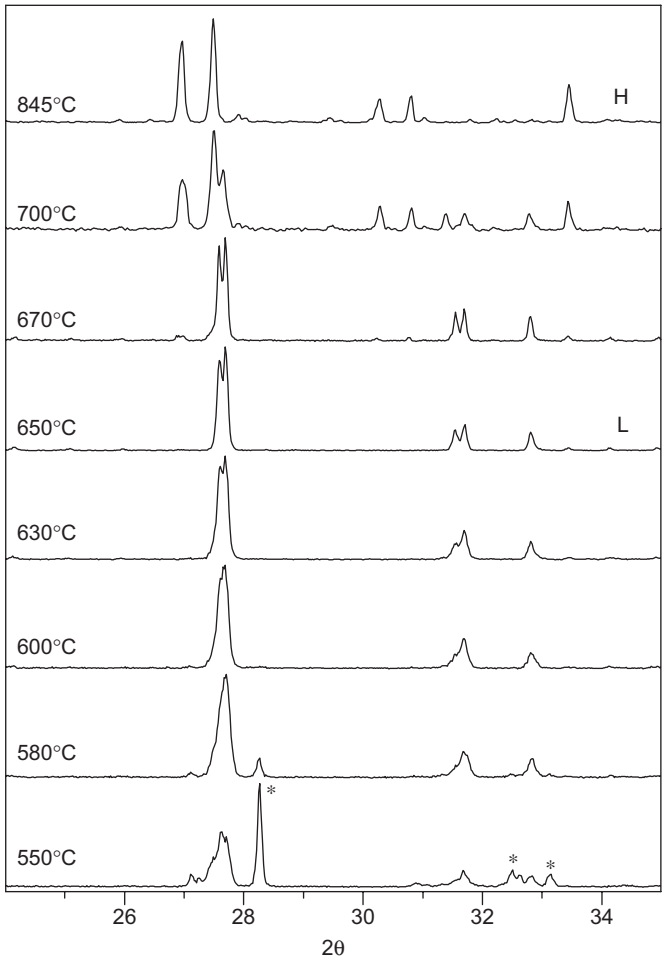

Fig. 1. XRD patterns of the precursor with composition Bi/Mo = 2.80 annealed at increasing temperatures * = ($\gamma(L)$-Bi_2MoO_6; L = low-temperature polymorph $Bi_{14}Mo_5O_{36}$; H = high-temperature polymorph $Bi_{14}Mo_5O_{36}$).

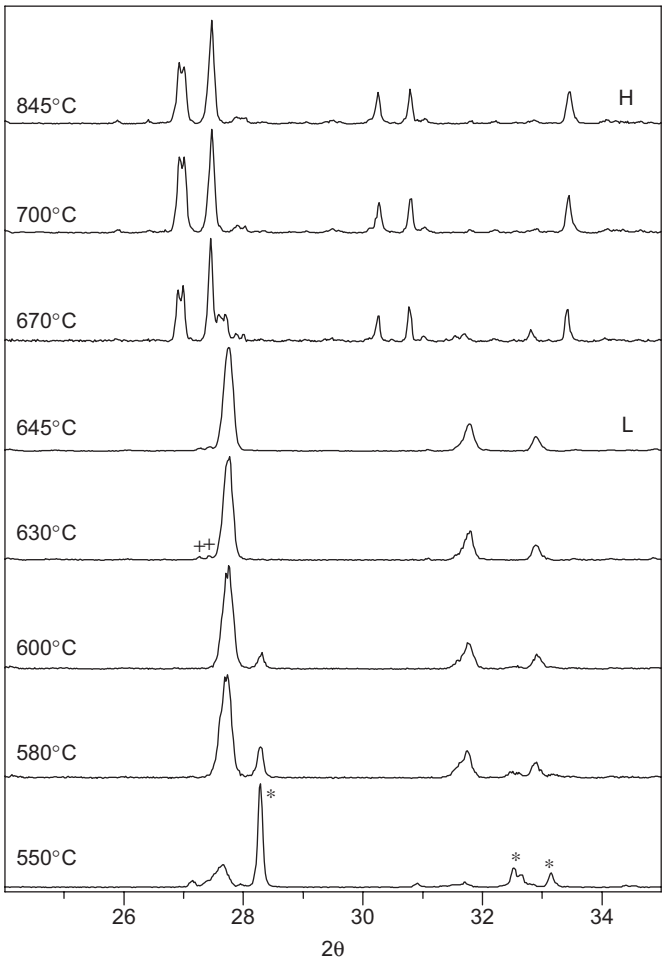

Fig. 2. XRD patterns of the precursor with composition Bi/Mo = 2.66 annealed at increasing temperatures * = ($\gamma(L)$-Bi_2MoO_6; + = $\gamma(H)$-Bi_2MoO_6; L = low temperature-polymorph $Bi_8Mo_3O_{21}$; H = high temperature-polymorph $Bi_8Mo_3O_{21}$).

for the particular case of Bi/Mo = 2.80. At temperatures up to 550 °C the formation of several oxides of bismuth and molybdenum occurs, including $\gamma(L)$–Bi_2MoO_6, which is the main crystalline phase at this temperature. Between 550 and 580 °C $\gamma(L)$ progressively disappears and a new compound starts to crystallize. At 600 °C the new oxide becomes the single phase, remaining stable up to 650 °C with an increase of the crystallinity. The new bismuth–molybdenum oxide must be formulated as $Bi_{14}Mo_5O_{36}$, the precursor Bi/Mo composition, since no weight losses were observed during thermal treatments, after evolution of H_2O, CO_2, NO and NO_2 at temperatures below 550 °C. At higher temperatures $Bi_{14}Mo_5O_{36}$ transforms to a high-temperature polymorph belonging to the well-known solid-solution of the $[Bi_{12}O_{14}]$ columnar phases [15,27,28].

In the same way, Fig. 2 reports the XRD showing the evolution of thermally annealed Bi/Mo = 2.66 precursor. As in the previous composition, a mixture of $\gamma(L)$–Bi_2MoO_6 with several bismuth–molybdenum oxides is observed up to 550 °C. At temperatures ranging from 580 to 630 °C the $\gamma(L)$ phase appears mixed with another new oxide, $\gamma(L)$ being only present as traces at 630 °C. The new oxide, which composition is $Bi_8Mo_3O_{21}$, becomes a single phase at 645 °C. Heating at higher temperatures allows the member of the solid-solution $[Bi_{12}O_{14}]$ columnar phase to be obtained. Similar to $Bi_{14}Mo_5O_{36}$ high-temperature phase, $Bi_8Mo_3O_{21}$ high-temperature polymorph appears as a unique phase from 700 °C.

In conclusion, and taking into account the results obtained by the authors in previous work [27,28], there exist four low-temperature stable-phases, in a very narrow composition range: $Bi_8Mo_3O_{21}$, $Bi_{14}Mo_5O_{36}$, $Bi_6Mo_2O_{15}$, $Bi_{10}Mo_3O_{24}$ with $m Bi_2O_3$:MoO_3 ratios 1.333, 1.400, 1.500 and 1.666, respectively. Intermediate compositions give rise to different mixture of phases. All these oxides start to transform, at temperatures of 650 °C or higher, to single phases of the so-called $[Bi_{12}O_{14}]$ columnar structural-type solid-solution, with the exception of $Bi_{10}Mo_3O_{24}$, which decomposes to a mixture of the columnar phase and $Bi_{38}Mo_7O_{78}^{12}$.

The morphology and crystal size of both new low-temperature phases, $Bi_{14}Mo_5O_{36}$ and $Bi_8Mo_3O_{21}$, were

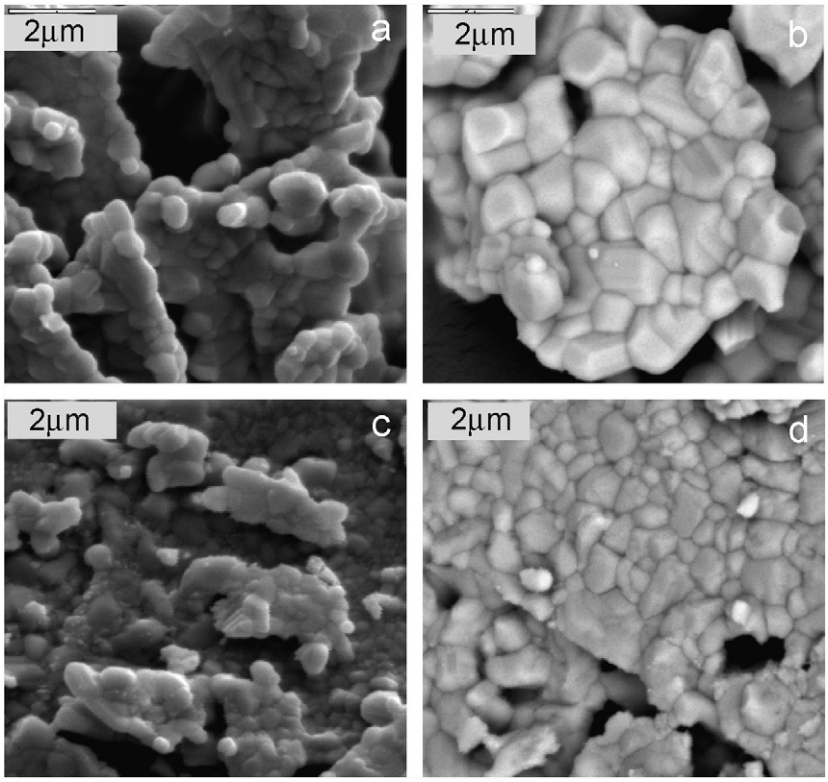

Fig. 3. SEM micrographs of the $Bi_{14}Mo_5O_{36}$ and $Bi_8Mo_3O_{21}$ phases obtained at different temperatures: $Bi_{14}Mo_5O_{36}$ at 600 °C (a) and 650 °C (b); $Bi_8Mo_3O_{21}$ at 600 °C (c) and 640 °C (d).

studied by scanning electron microscopy at different temperatures. The single phase $Bi_{14}Mo_5O_{36}$, obtained at 600 °C (Fig. 3a), consists in a very homogeneous powder with spherical particles of diameter between 0.5 and 1 μm. In the scanning electron micrograph of this compound annealed at 650 °C (Fig. 3b) the biggest change observed correspond to the increase in size of grains that reach 1.5–2 μm, with parallelepipedal shape. On the contrary, in the $Bi_8Mo_3O_{21}$ phase obtained at 600 °C (Fig. 3c), two kinds of particles can be observed: conglomerates of fine particles, and larger grains with spherical shape, 0.2–0.7 μm in size. This result agrees with the XRD data, since a mixture of $Bi_8Mo_3O_{21}$ and $\gamma(L)$–Bi_2MoO_6 was observed at the same temperature. When the sample is annealed to 640 °C, it becomes a homogeneous powder, constituted by irregular parallelepipedal grains of different sizes, ranging between 0.2 and 1.5 μm (Fig. 3d).

The ab initio structural study of the low-temperature polymorphs of $Bi_{10}Mo_3O_{24}$ and $Bi_6Mo_2O_{15}$ seems to point to a structural relationship between these phases and the columnar $[Bi_{12}O_{14}]$ structures, and hence to the fluorite framework. On the other hand, XRD shows the similarities and connections between the XRD patterns of the four low-temperature mixed oxides mentioned. Therefore, it is interesting to undertake a similar study on the new synthesized $Bi_{14}Mo_5O_{36}$ and $Bi_8Mo_3O_{21}$ low-temperature polymorphs, in order to ascertain if such relation remains constant over all the series. Crystalline phases were isolated by successive heating runs (10 h each) from 450 to 600 °C, every 50 °C, and then every 10 °C up to 650 and 645 °C for $Bi_{14}Mo_5O_{36}$ and $Bi_8Mo_3O_{21}$, respectively.

The method to determine the crystal data of both $Bi_{14}Mo_5O_{36}$ and $Bi_8Mo_3O_{21}$ oxides was reported elsewhere [27]. The final lattice parameters determined for both phases are reported in Table 1, together with those of the low-temperature polymorphs of $Bi_{10}Mo_3O_{24}$ and $Bi_6Mo_2O_{15}$, and the high-temperature polymorph of $Bi_6Mo_2O_{15}$, which belongs to the so-called solid solution $[Bi_{12}O_{14}]$ columnar phases [27]. C-centring lattices for $Bi_{10}Mo_3O_{24}$ and $Bi_{14}Mo_5O_{36}$ were suggested by Fig. 8, see later on, and confirmed by unit cell parameters refinements. Fig. 4 presents the XRD patterns of the four low temperature phases plus the $\gamma(H)$-Bi_2MoO_6 one. Fig. 5 shows the indexed XRD patterns of both $Bi_{14}Mo_5O_{36}$ and $Bi_8Mo_3O_{21}$ low-temperature phases. It is worth noting the similarities between the b and c parameters of four phases, while a monotonic increase of a unit-cell parameter and β angle is observed as the Bi/Mo ratio decreases. This fact again points to the close relationship between the frameworks of these phases, all very similar, and those of the so-called $[Bi_{12}O_{14}]$ columnar compounds, previously suggested by the authors [27,28].

The volumic masses measured for these phases are also reported in Table 1, showing very good agreement with the calculated values, assuming 2 formula units per cell for all the phases.

A study by electron diffraction was undertaken in order to better understand the above-mentioned structural

Table 1
Crystal data of low-temperature stable-polymorphs of the $Bi_{2n+4}Mo_nO_{6(n+1)}$ series and the high-temperature polymorph of $Bi_{12}Mo_4O_{30}$ (H–$Bi_{12}Mo_4O_{30}$)

Compound	$Bi_{10}Mo_3O_{24}$ ($n=3$)	$Bi_{12}Mo_4O_{30}$ ($n=4$)	$Bi_{14}Mo_5O_{36}$ ($n=5$)	$Bi_{16}Mo_6O_{42}$ ($n=6$)	H–$Bi_{12}Mo_4O_{30}$
a (Å)	23.7235(4)	29.0674(4)	34.476(2)	39.97(2)	11.7451(9)
b (Å)	5.64720(8)	5.64795(7)	5.6414(3)	5.632(4)	5.8010(4)
c (Å)	8.6798(1)	8.6620(1)	8.6433(4)	8.634(4)	24.795(2)
β (º)	95.879(1)	97.979(1)	99.690(5)	101.02(2)	102.910(7)
V (Å^3)	1156.7	1408.3	1657.1	1907.6	1646.7
S.G	C2, Cm, C2/m	Pa, P2/a	C2, Cm, C2/m	Pa, P2/a	P2/c
ρ_x (g cm^{-3})	7.93	7.95	7.98	7.99	6.79
ρ_{exp} (g cm^{-3})	7.90(1)	8.01(2)	7.98(3)	7.94(1)	
Z	2	2	2	2	2
References	[28]	[27]	This work	This work	[27]

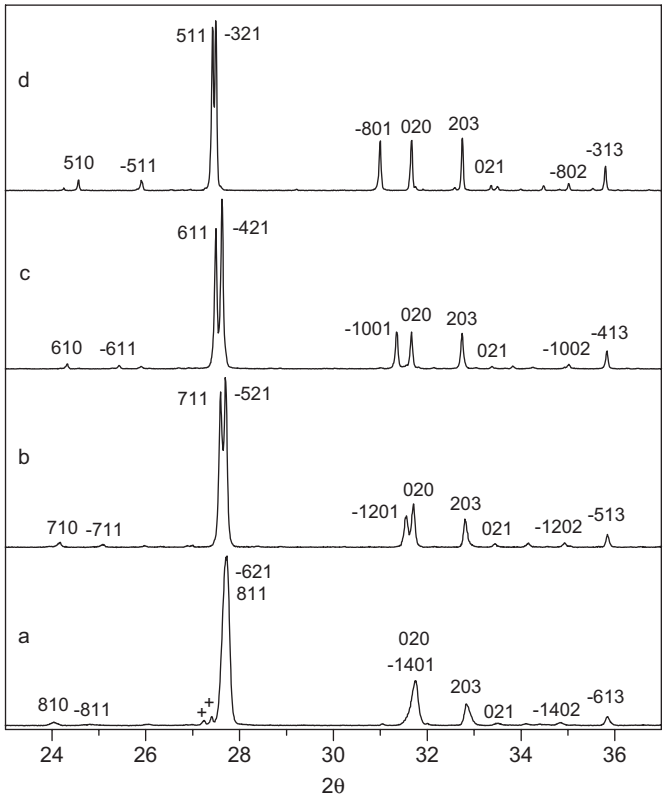

Fig. 4. XRD patterns of the low-temperature phases: (a) $Bi_8Mo_3O_{21}$, (b) $Bi_{14}Mo_5O_{36}$, (c) $Bi_6Mo_2O_{15}$ and (d) $Bi_{10}Mo_3O_{24}$ ($\gamma(H)$-Bi_2MoO_6).

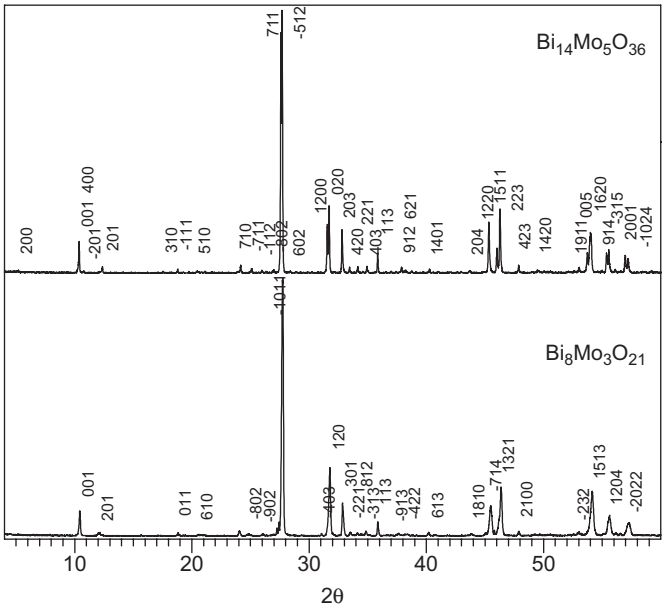

Fig. 5. Indexed XRD patterns of bismuth–molybdenum oxides $Bi_{14}Mo_5O_{36}$ and $Bi_8Mo_3O_{21}$ (low-temperature polymorphs).

relationship of the new low-temperature Bi–Mo oxides with the fluorite framework. The reciprocal lattice of the four samples was studied by systematic tilting in the $\pm 45^\circ$ double-tilting holder of the JEM 2000FXII sample holder and approximate unit cells were obtained from the selected area electron diffraction (SAED) patterns, which are in very good agreement with the values determined by XRD (Table 1).

In Fig. 6 the SAED patterns along the short axis of the four samples are collected. This figure clearly indicates the homologous-series character of this sample series, since all the diffraction patterns show very similar characteristics. The more intense diffraction maxima are related with the basic fluorite-type subcell reflections in the [010] zone axis. The weaker reflections correspond in all cases to a superstructure along the $[602]_F$ fluorite direction. The (200) spacing for these superlattices is:

$Bi_{10}Mo_3O_{24}$: $(200) = 13 \times (602)_F$,
$Bi_6Mo_2O_{15}$: $(200) = 16 \times (602)_F$,
$Bi_{14}Mo_5O_{36}$: $(200) = 19 \times (602)_F$,
$Bi_8Mo_3O_{21}$: $(200) = 22 \times (602)_F$.

The length of the c-axis is related to fluorite spacing as:

$Bi_{10}Mo_3O_{24}$: $(001) = 13 \times (-208)_F$,
$Bi_6Mo_2O_{15}$: $(001) = 16 \times (-2010)_F$,
$Bi_{14}Mo_5O_{36}$: $(001) = 19 \times (-2012)_F$,
$Bi_8Mo_3O_{21}$: $(001) = 22 \times (-2014)_F$.

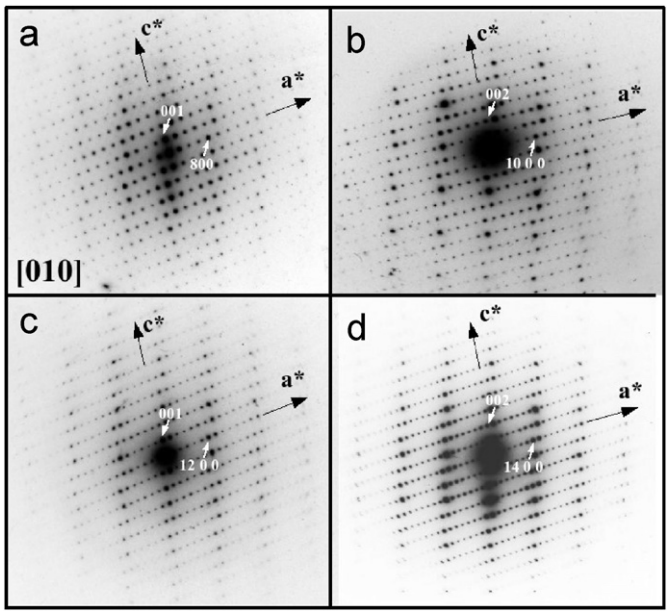

Fig. 6. Selected area electron diffraction patterns of the samples $Bi_{10}Mo_3O_{24}$ (a), $Bi_6Mo_2O_{15}$ (b), $Bi_{14}Mo_5O_{36}$ (c), and $Bi_8Mo_3O_{21}$ (d) oriented along the short axis *b*.

Although the 0 0 1 reflection maintains an almost constant modulus, it slowly changes its relationship with the basic fluorite sublattice.

A different and unified way to describe the whole series is using the modulated structure approach, where we consider a basic subcell derived from fluorite with modulation satellites [30,31]. The reciprocal lattice is then described as $\mathbf{G} = h\mathbf{a}^* + k\mathbf{b}^* + l\mathbf{c}^* + mq$, $\mathbf{a}^*$, $\mathbf{b}^*$ and $\mathbf{c}^*$ being a basis of the reciprocal lattice, m an integer number and q the modulation vector defined as $\mathbf{q} = \gamma(602)^*$. The value of γ could possibly change continuously, but only the values of 1/13, 1/16, 1/19 and 1/22, those corresponding to the described superstructures, have been found. Although these numbers may look a bit whimsy, they make more sense when one looks at the schemes depicted in Fig. 7. In Fig. 7(a), a scheme of the [010] electron diffraction pattern of the phase $Bi_{10}Mo_3O_{24}$ is represented. The $\mathbf{q}$ vector is represented in the diagram according to its definition as $\mathbf{q} = 1/13(602)^*$. It can be easily seen that with only one $\mathbf{q}$ vector we can generate the whole reciprocal lattice from the basic fluorite sublattice. The same happens for the three other phases, see Figs. 7(b)–(d). From these schemes and their relationships between the $\mathbf{q}$ vector and the basic fluorite sublattice it becomes clear that these four cases correspond to consecutive terms of a homologous series. These relations can be also envisaged in the superlattice–sublattice relation matrices shown below, obtained from the indexing of the observed SAED patterns, relating the hkl Miller indices of both sublattices in the different phases:

$$Bi_{10}Mo_3O_{24}: \quad \begin{pmatrix} h_M \\ k_M \\ l_M \end{pmatrix} = \begin{pmatrix} 6/26 & 0 & 2/26 \\ 0 & 1 & 0 \\ -2/13 & 0 & 8/13 \end{pmatrix} \begin{pmatrix} h_F \\ k_F \\ l_F \end{pmatrix},$$

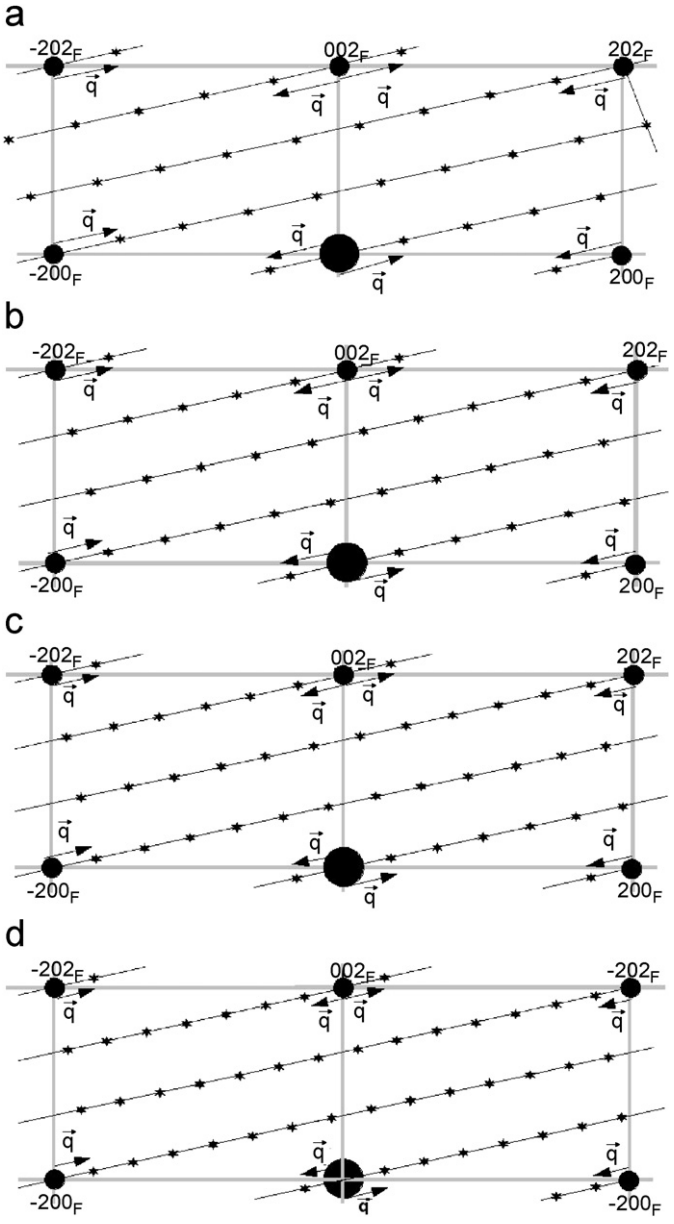

Fig. 7. Schematized SAED patterns along [010] of samples $Bi_{10}Mo_3O_{24}$ (a), $Bi_6Mo_2O_{15}$ (b), $Bi_{14}Mo_5O_{36}$ (c) and $Bi_8Mo_3O_{21}$ (d). Black circles indicate the basic fluorite reflections and black stars represent the superlattice reflections. The $\mathbf{q}$ vectors are also depicted.

$$Bi_6Mo_2O_{15}: \quad \begin{pmatrix} h_M \\ k_M \\ l_M \end{pmatrix} = \begin{pmatrix} 6/32 & 0 & 2/32 \\ 0 & 1 & 0 \\ -2/16 & 0 & 10/16 \end{pmatrix} \begin{pmatrix} h_F \\ k_F \\ l_F \end{pmatrix},$$

$$Bi_{14}Mo_5O_{36}: \quad \begin{pmatrix} h_M \\ k_M \\ l_M \end{pmatrix} = \begin{pmatrix} 6/38 & 0 & 2/38 \\ 0 & 1 & 0 \\ -2/19 & 0 & 12/19 \end{pmatrix} \begin{pmatrix} h_F \\ k_F \\ l_F \end{pmatrix},$$

$$\mathrm{Bi_8Mo_3O_{21}}: \quad \begin{pmatrix} h_M \\ k_M \\ l_M \end{pmatrix} = \begin{pmatrix} 6/44 & 0 & 2/44 \\ 0 & 1 & 0 \\ -2/22 & 0 & 14/22 \end{pmatrix} \begin{pmatrix} h_F \\ k_F \\ l_F \end{pmatrix},$$

where the subindices M and F stand for monoclinic and fluorite, respectively. The same matrices relate the reciprocal parameters.

From these matrices we can obtain those relating the lattice basis vectors with the transpose of the inverse matrices:

$$\mathrm{Bi_{10}Mo_3O_{24}}: \quad \begin{pmatrix} \vec{a}_M \\ \vec{b}_M \\ \vec{c}_M \end{pmatrix} = \begin{pmatrix} 4 & 0 & 1 \\ 0 & 1 & 0 \\ -1/2 & 0 & 3/2 \end{pmatrix} \begin{pmatrix} \vec{a}_F \\ \vec{b}_F \\ \vec{c}_F \end{pmatrix},$$

$$\mathrm{Bi_6Mo_2O_{15}}: \quad \begin{pmatrix} \vec{a}_M \\ \vec{b}_M \\ \vec{c}_M \end{pmatrix} = \begin{pmatrix} 5 & 0 & 1 \\ 0 & 1 & 0 \\ -1/2 & 0 & 3/2 \end{pmatrix} \begin{pmatrix} \vec{a}_F \\ \vec{b}_F \\ \vec{c}_F \end{pmatrix},$$

$$\mathrm{Bi_{14}Mo_5O_{36}}: \quad \begin{pmatrix} \vec{a}_M \\ \vec{b}_M \\ \vec{c}_M \end{pmatrix} = \begin{pmatrix} 6 & 0 & 1 \\ 0 & 1 & 0 \\ -1/2 & 0 & 3/2 \end{pmatrix} \begin{pmatrix} \vec{a}_F \\ \vec{b}_F \\ \vec{c}_F \end{pmatrix},$$

$$\mathrm{Bi_8Mo_3O_{21}}: \quad \begin{pmatrix} \vec{a}_M \\ \vec{b}_M \\ \vec{c}_M \end{pmatrix} = \begin{pmatrix} 7 & 0 & 1 \\ 0 & 1 & 0 \\ -1/2 & 0 & 3/2 \end{pmatrix} \begin{pmatrix} \vec{a}_f \\ \vec{b}_F \\ \vec{c}_F \end{pmatrix}.$$

These structural relationships show that there exist a continuous series of phases, with general formula

$\mathrm{Bi_{2n+4}Mo_nO_{6(n+1)}}$,

where $n=3$ for $\mathrm{Bi_{10}Mo_3O_{24}}$, $n=4$ for $\mathrm{Bi_6Mo_2O_{15}}$ (or $\mathrm{Bi_{12}Mo_4O_{30}}$), $n=5$ for $\mathrm{Bi_{14}Mo_5O_{36}}$ and $n=6$ for $\mathrm{Bi_8Mo_3O_{21}}$. The space groups of their monoclinic crystal structures must be C2, Cm or C2/m for odd values of n, and Pa or P2/a for n even ones. The unit cells of the terms of the series are given by

$$\begin{pmatrix} \vec{a}_M \\ \vec{b}_M \\ \vec{c}_M \end{pmatrix} = \begin{pmatrix} n+1 & 0 & 1 \\ 0 & 1 & 0 \\ -1/2 & 0 & 3/2 \end{pmatrix} \begin{pmatrix} \vec{a}_F \\ \vec{b}_F \\ \vec{c}_F \end{pmatrix}.$$

Notice that all the matrix elements remain unaltered except for the first one, which take values of 4, 5, 6 and 7 for the four different phases. This value, $n+1$, is related with the superlattices term by the expression $3(n+1)+1$, so the term $n=3$ accounts for the 13-fold, $n=4$ for the 16-fold, $n=5$ for the 19-fold and $n=6$ for the 22-fold superstructures (the inverse of the above mentioned γ values).

The relationship between the layout of heavy atoms in the fluorite structure and the low-temperature bismuth–molybdenum oxides can be easily viewed in Fig. 8. This figure suggest that the unit cells of $n=3$ ($\mathrm{Bi_{10}Mo_3O_{24}}$) and $n=5$ ($\mathrm{Bi_{14}Mo_5O_{36}}$) superstructures should be C-centered, as it is confirmed by the indexation of the X-ray diffraction patterns. For comparative purpose, the cell of a high-temperature term of the solid-solution [$\mathrm{Bi_{12}O_{14}}$] columnar phases has been also included.

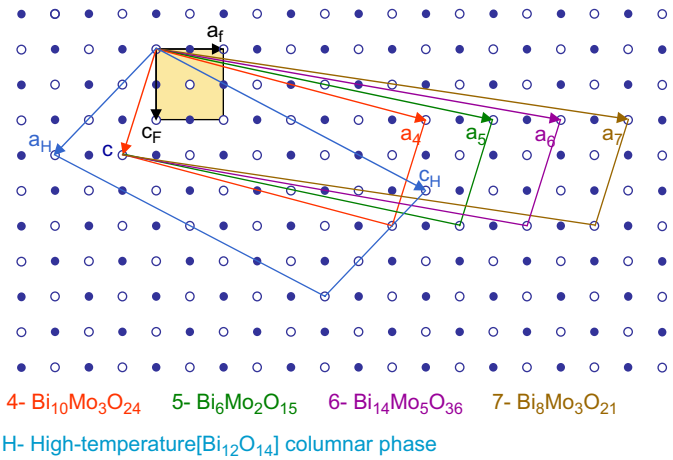

Fig. 8. Structural relationship between the layout of heavy atoms in the fluorite structure and $\mathrm{Bi_8Mo_3O_{21}}$, $\mathrm{Bi_{14}Mo_5O_{36}}$, $\mathrm{Bi_6Mo_2O_{15}}$ and $\mathrm{Bi_{10}Mo_3O_{24}}$ low-temperature oxides, and one term of the high-temperature solid-solution [$\mathrm{Bi_{12}O_{14}}$] columnar phases.

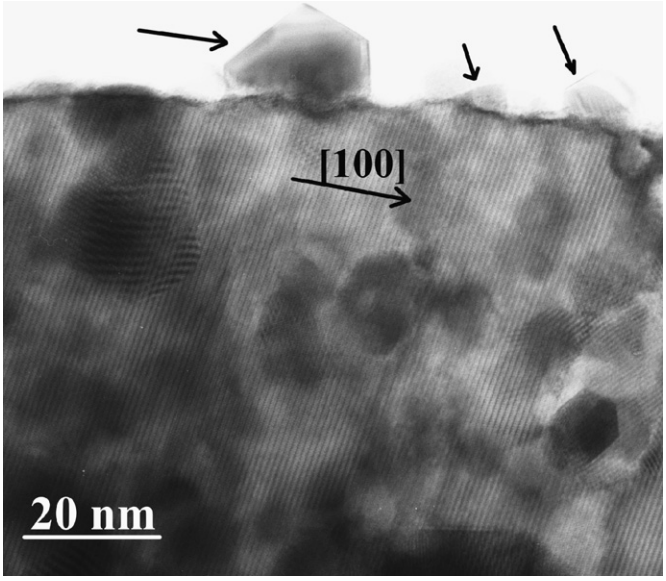

Fig. 9. Electron micrograph from a $\mathrm{Bi_{10}Mo_3O_{24}}$ crystal oriented along [010]. Notice the periodic arrangement of the lattice planes and the presence of $\mathrm{Bi_2O_3}$ nanocrystals decorating the surface of the crystal, generated by electron beam damage.

In Fig. 9 we present a transmission electron micrograph of sample $\mathrm{Bi_{10}Mo_3O_{24}}$ showing a periodic arrangement of lattice planes without defects. The crystals are not completely stable and exude small crystallites, possibly $\mathrm{Bi_2O_3}$, after prolonged exposure to the electron beam, due to electron beam radiation damage.

In order to compare the conductivity behaviour of the two new low-temperature phases reported in this work with that of the closely related $\mathrm{Bi_{10}Mo_3O_{24}}$ and $\mathrm{Bi_6Mo_2O_{15}}$ oxides, a study of their electrical conductivity was performed on $\mathrm{Bi_{14}Mo_5O_{36}}$ and $\mathrm{Bi_8Mo_3O_{21}}$ materials.

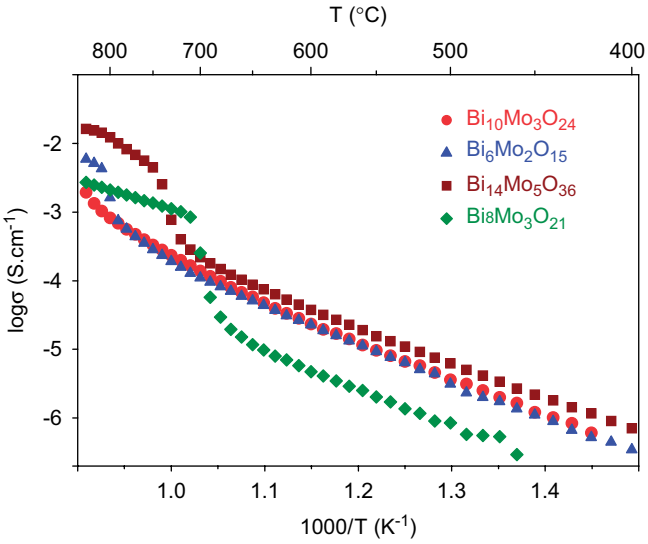

Fig. 10. Conductivity (σ) vs. reciprocal temperature for $Bi_{10}Mo_3O_{24}$, $Bi_6Mo_2O_{15}$, $Bi_{14}Mo_5O_{36}$ and $Bi_8Mo_3O_{21}$.

Experimental conductivity values were fitted to an Arrhenius plot for the four materials, as can be observed in Fig. 10. From the plots in the heating runs it is possible to draw different slopes for all phases. As the authors have previously reported [27,28], the two richest bismuth phases, $Bi_{10}Mo_3O_{24}$ and $Bi_6Mo_2O_{15}$, exhibit smooth slope changes at 650 and 670 °C, respectively, which cannot be attributed to clear structural changes, whereas an abrupt slope change occurs at 820 °C for $Bi_{10}Mo_3O_{24}$, and between 785 and 805 °C for $Bi_6Mo_2O_{15}$. These high-temperature effects correspond to the total transition of the low-temperature polymorph to the high-temperature form for $Bi_6Mo_2O_{15}$ or the decomposition of $Bi_{10}Mo_3O_{24}$ oxide to a mixture of $Bi_{38}Mo_7O_{78}$ with high-temperature phases belonging to the $[Bi_{12}O_{14}]$ columnar family. However for the two new phases, $Bi_{14}Mo_5O_{36}$ and $Bi_8Mo_3O_{21}$, two well-defined linear dependencies are observed. In the case of $Bi_{14}Mo_5O_{36}$ the first linear dependency persists to about 665 °C when the transition to a different behavior starts, reaching some degree of linearity at the end of the experiment, at about 800 °C. This transition agrees perfectly with that observed by XRD from low to high-temperature polymorphs (Fig. 1). For the bismuth-poor phase, $Bi_8Mo_3O_{21}$, a similar behavior is observed, but at quite different transition temperatures: the low-temperature linearity arrives at 645 °C, with a second linear behavior reached at 710 °C, corresponding to the high-temperature polymorph of the same composition, also belonging to the $[Bi_{12}O_{14}]$ columnar family, as XRD results show (Fig. 2).

The measured activation energies for the four low-temperature bismuth–molybdenum oxides is similar: 1.29, 1.20, 1.07 and 1.12 eV for $Bi_{10}Mo_3O_{24}$, $Bi_6Mo_2O_{15}$, $Bi_{14}Mo_5O_{36}$ and $Bi_8Mo_3O_{21}$, respectively, and also similar is their ionic conductor quality. The lower thermal stability of the low temperature $Bi_8Mo_3O_{21}$ allows the poorest conductivity values to be reached for this phase.

4. Conclusions

The so-called *n*-butylamine wet-synthesis method, applied to mixtures of $Bi(NO_3)\cdot 5H_2O$ and MoO_3 (Bi/Mo ratios ranging between 2/1 and 3/1), led to very reactive precursors. Several annealings, at very precise temperatures, allow four low-temperature single phases to be isolated, with close Bi/Mo ratios and compositions: $Bi_8Mo_3O_{21}$, $Bi_{14}Mo_5O_{36}$, $Bi_6Mo_2O_{15}$ and $Bi_{10}Mo_3O_{24}$. The thermal stability of these oxides is lower as Bi/Mo ratio decreases, transforming to the corresponding high-temperature polymorphs, which belong to the so-called $[Bi_{12}O_{14}]$ columnar-structural type. The most stable phase is $Bi_{10}Mo_3O_{24}$, which does not transform to a high-temperature polymorph but decomposes to a mixture of $Bi_{38}Mo_7O_{78}$ and a columnar phase.

X-ray diffraction and electron microscopy studies have demonstrated the structural relationship of this whole series of oxides with the $[Bi_{12}O_{14}]$ columnar-structural type and hence, with the fluorite framework. Therefore these oxides constitute a homologous series, which structures can be described as superstructures of the fluorite subcell.

Impedance spectroscopy measurements have also shown that all these materials are quite good ionic conductors, with similar response in their whole range of stability. Moreover, these results confirm the structural transitions observed at high temperatures by X-ray powder diffraction.

Acknowledgments

The authors want to thank the financial support given by the Spanish MEC (MAT2004-00868 project).

References

[1] R.S. Roth, T.L. Waring, J. Res. Nat. Bur. Stand. A 66 (1962) 451–463.
[2] W. Zhou, D.A. Jefferson, M.A. Alario-Franco, J.M. Thomas, J. Phys. Chem. 91 (1987) 512–514.
[3] R. Miida, M. Tanaka, Jpn J. Appl. Phys. 29 (1990) 1132–1138.
[4] C.D. Ling, R.L. Withers, S. Schmid, J.G. Thompson, J. Solid State Chem. 137 (1998) 42–61.
[5] C.D. Ling, J. Solid State Chem. 148 (1999) 380–405.
[6] U. Pirnat, M. Valant, B. Jancar, D. Suvorov, Chem. Mater. 17 (2005) 5155–5160.
[7] J.F. Brazdil, D.D. Suresh, R.K. Grasselli, J. Catal. 66 (1980) 347–367.
[8] D.H. Galvan, S. Fuentes, M. Avalos-Borja, L. Cota-Araiza, E.A. Early, M.B. Maple, J. Cruz-Reyes, J. Phys. Condens. Matter. 5 (1993) A217–A218.
[9] D.D. Agarwal, K.L. Madhok, H.S. Goswami, React. Kin. Catal. Lett. 52 (1994) 225–232.
[10] T.E. Crumpton, M.G. Francesconi, C. Greaves, J. Solid State Chem. 175 (2003) 197–206.
[11] M. Valldor, S. Esmaeilzadeh, C. Pay-Gomez, J. Grins, J. Solid State Chem. 152 (2000) 573–576.
[12] D.J. Buttrey, D.A. Jefferson, J.M. Thomas, Mater. Res. Bull. 21 (1986) 739–744.
[13] G. Spinolo, C. Tomasi, Powder Diffr. 12 (1997) 16–19.
[14] R. Kohlmuller, J.P. Badaud, Bull. Soc. Chim. France 10 (1969) 3434.
[15] D.J. Buttrey, T. Vogt, G.P.A. Yap, A.L. Rheingold, Mat. Res. Bull. 32 (1997) 947–963.

[16] R. Enjalbert, G. Hasselmann, J. Galy, J. Solid State Chem. 131 (1997) 236–245.
[17] H.-Y. Chen, A.W. Sleight, J. Solid State Chem. 63 (1986) 70–75.
[18] F. Theobald, A. Laarif, A.W. Hewat, Mater. Res. Bull. 20 (1985) 653.
[19] D.J. Buttrey, D.A. Jefferson, J.M. Thomas, Philos. Mag. A 53 (1986) 897.
[20] D.J. Buttrey, T. Vogt, U. Wildgruber, W.R. Robinson, J. Solid State Chem. 111 (1994) 118–127.
[21] J. Galy, R. Enjalbert, P. Millán, A. Castro, C. R. Acad. Sci. Paris 317 Série II (1993) 43.
[22] A. Castro, P. Millán, J. Ricote, L. Pardo, J. Mater. Chem. 10 (2000) 767–771.
[23] K. Shantha, G.N. Subbanna, K.B.R. Varma, J. Solid State Chem. 142 (1999) 41–47.
[24] A. Castro, D. Palem, J. Mater. Chem. 12 (2002) 2774–2780.
[25] W.T. Jeong, K.S. Lee, J. Alloy. Compd. 322 (2001) 205–210.
[26] J.M. González-Calbet, J. Alonso, E. Herrero, M. Vallet-Regí, Solid State Ion. 101/103 (1997) 119–123.
[27] E. Vila, J.M. Rojo, J.E. Iglesias, A. Castro, Chem. Mater. 16 (2004) 1732–1739.
[28] E. Vila, J.E. Iglesias, J. Galy, A. Castro, Solid State Sci 7 (2005) 1369–1376.
[29] J. Galy, R. Enjalbert, P. Rozier, P. Millet, Solid State Sci. 5 (2003) 165–174.
[30] R.L. Withers, Prog. Cryst. Growth Charact. 18 (1989) 139–204.
[31] R.L. Withers, S. Schmid, J.G. Thompson, Prog. Solid State Chem. 26 (1998) 1–96.